

MASTER OT J030227.28+191754.5: a dwarf nova at a massive oxygen-neon white-dwarf system ?

MARIKO KIMURA,¹ KAZUMI KASHIYAMA,^{2,3} TOSHIKAZU SHIGEYAMA,⁴ YUSUKE TAMPO,⁵ SHINYA YAMADA,⁶ AND TERUAKI ENOTO^{1,7}

¹*Cluster for Pioneering Research,
Institute of Physical and Chemical Research (RIKEN),
2-1 Hirosawa, Wako, Saitama 351-0198, Japan*

²*Astronomical Institute, Tohoku University,
Sendai 980-8578, Japan*

³*Kavli Institute for the Physics and Mathematics of the Universe,
The University of Tokyo, Kashiwa 277-8583, Japan*

⁴*Research Center for the Early Universe,
Graduate School of Science, University of Tokyo,
Bunkyo-ku, Tokyo 113-0033, Japan*

⁵*Department of Astronomy, Graduate School of Science,
Kyoto University, Kitashirakawa-Oiwake-cho, Sakyo-ku,
Kyoto 606-8502, Japan*

⁶*Department of Physics, Rikkyo University,
3-34-1 Nishi-Ikebukuro, Toshima-ku, Tokyo 171-8501, Japan*

⁷*Department of Physics, Graduate School of Science,
Kyoto University, Kitashirakawa-Oiwake-cho, Sakyo-ku,
Kyoto 606-8502, Japan*

ABSTRACT

We present timing and spectral analysis results of the *NICER* and *NuSTAR* observations of the dwarf nova MASTER OT J030227.28+191754.5 during the 2021–2022 outburst. The soft X-ray component was found to be dominated by blackbody radiation with a temperature of ~ 30 eV and also showed prominent oxygen and neon emission lines. The blackbody luminosity exceeded 10^{34} ergs s⁻¹, which is consistent with theoretical predictions, and then decreased more than an order of magnitude in 3.5 days. The inferred abundances of oxygen and neon in the optically-thin coronal region surrounding the central white dwarf (WD) are several times higher than the respective solar values. Although inconclusive, the abundance enrichment may originate from the WD, indicating that it may be mainly composed of oxygen and neon. Assuming that the blackbody radiation comes from the belt-shaped boundary layer between the WD and the accretion disk, we estimated the WD radius to be $(2.9 \pm 1.1) \times 10^8$ cm, which corresponds to the WD mass range of 1.15–1.34 M_{\odot} . If the accretion continues for another \sim Gyr, the WD may experience an accretion-induced collapse into a neutron star and form a so-called black-widow pulsar system.

Keywords: Cataclysmic variable stars (203) — Dwarf novae (418) — X-ray sources (1822) — Stellar accretion disks (1579) — WZ Sagittae stars (1809)

1. INTRODUCTION

MASTER OT J030227.28+191754.5 = AT2021afpi = PNV J03022732+1917552 (hereafter referred to as MASTER J0302) is the cataclysmic variable (CV) that entered an outburst at the end of 2021 November. It was discovered on November 26.82568 UT (Zhirkov et al. 2021) as a possible optical counterpart of the neutrino event IceCube-211225A, which occurred at 06:22:21.56

UT on November 25 (Lagunas 2021). Subsequently, an X-ray observation of the object was made on November 28 and a significant brightening was detected (Paliya 2021).

According to the Central Bureau for Astronomical Telegrams (CBAT), the object had been fainter than 16 mag on November 23.7421 UT before the outburst. Its optical magnitude at the outburst maximum was 11.4

mag in the V band (Tampo et al. in prep.), whereas the quiescent optical magnitude is 21.94(7) in the g' band (Ahumada et al. 2020). The large-amplitude outburst and detection of the initial optical spectrum dominated by a blue continuum with strong single-peaked emission lines are initially believed to indicate that this object would be a classical He/N nova (Stein et al. 2021; Boettcher et al. 2022). However, the object was later identified as a WZ Sge-type system, a subclass of dwarf novae (DNe) in further follow-up optical spectroscopy and photometry (Isogai et al. 2021).

The DN is a subgroup of CVs, which is a close binary system composed of a “primary” of white dwarf (WD) and a “secondary” of low-mass star. The WD in a CV is surrounded by an accretion disk formed by the transferred mass from the secondary star (Warner 1995). The accretion rate from the disk to the WD is low in the quiescent state. Due to thermal instability in the accretion disk, the accretion rate becomes high, and DNe show sudden brightening in the disk, which is called an outburst (Osaki 1996, 2005). WZ Sge-type DNe are characterized by large-amplitude (typically 6–9 mag) outbursts, rebrightening after a main outburst, and short-term optical modulations, such as early and ordinary superhumps, during outbursts (see Kato 2015, for a review). Their binary mass ratio ($q \equiv M_2/M_1$, where M_1 and M_2 are the masses of the primary and secondary stars, respectively) is extremely low, ≤ 0.08 . Isogai et al. (2021) reported the emergence of early superhumps two days after the outburst maximum (see the left panel of Figure A1). Early superhumps appear when the disk radius exceeds the 2:1 resonance radius, which is ~ 1.5 -times larger than the disk radius in quiescence (Osaki & Meyer 2002). At the onset of the thermal instability, the disk expands because of the angular momentum transfer from the inner part of the disk to its outer part. The emergence of early superhumps is evidence of a sudden increase in the mass accretion rate. At that time, double-peaked emission lines from the disk were also observed in the optical spectrum (see the right panel of Figure A1). These two observations identified MASTER J0302 as a DN.

The identification as a DN is not consistent with the neutrino detection (IceCube-211225A) in the current DN and neutrino-emission models, though potential neutrino emission from a classical nova is proposed (Guetta et al. 2023; Bednarek & Śmiałkowski 2022). In fact, MASTER J0302 brightened in the optical band 8.5 hours before the IceCube event (Sarneczky et al. 2021), and thus they must not be associated. Two bright AGNs were listed later as the possible counterpart of IceCube-211225A (Kadler et al. 2021). In addition, γ -ray obser-

vations reported no significant event (Quinn et al. 2021; Ayala 2021); the fact is consistent with the identification of MASTER J0302 as a DN and not as a neutrino event, which is often associated with gamma-ray events. As such, IceCube-211225A is currently believed not to originate from MASTER J0302.

Although previous studies of DNe have elucidated their optical properties, many unsolved problems remain in their X-ray properties. What we know about the X-ray properties and what we don’t are briefly summarized below. In the current standard model of the DN, its X-ray emitting plasma is located in the vicinity of the WD and is powered by accretion. When the system enters an outburst, the accretion rate becomes higher than usual so that the total energy released by accretion becomes larger. During the outburst, the optically-thin X-ray plasma in quiescence becomes optically thick (Patterson & Raymond 1985a; Narayan & Popham 1993; Patterson & Raymond 1985b). As a result, the X-ray luminosity in general decreases during the outburst and in contrast, the extreme-ultra-violet (EUV) luminosity increases. However, several DNe have been reported to show an increase in X-ray flux during outbursts, and WZ Sge-type DNe belong to these outliers (Wheatley & Mauche 2005; Byckling et al. 2009; Neustroev et al. 2018). Although a naive expectation from the standard model is that the observed high X-ray flux during outbursts may be attributed to soft X-rays radiated from the optically-thick boundary layer, which would be a blackbody emission with a temperature of several tens of eV, such blackbody emissions were observed only in a handful of objects during outbursts (Mauche 2004; Byckling et al. 2009). In general, the observed soft X-ray luminosity during outbursts is more than 100 times weaker than the prediction. This “missing boundary-layer problem” proposed by Ferland et al. (1982) four decades ago remains unsolved so far.

Another unsolved problem is the ultimate fate in the evolution of CVs. It has long been proposed that some CVs will eventually evolve into (neutron-star) low-mass X-ray binaries (Kulkarni & Narayan 1988); Observationally, WZ Sge-type DNe would be the best targets to constrain the hypothesis, given that WZ Sge-type DNe are believed to be the most evolved CV systems. In particular, their binary parameters are keys. WZ Sge-type DNe are too faint to observe during quiescence due to their low mass-transfer and mass-accretion rates. Their outbursts provide good opportunities for determining their binary parameters observationally. X-ray observations of WZ Sge-type DNe during their outbursts are no exceptions and they have two specific advantages: to tackle the missing boundary-layer problem through

search for the soft X-ray emission and to constrain the evolutionary path of CVs possibly by means of determination of the WD mass and/or abundances of elements in the high-temperature plasma.

MASTER J0302 showed the largest outburst among WZ Sge-type DNe and became brighter in X-rays during outburst, as other WZ Sge-type DNe do. Then, its 2021–2022 outburst provides us with a good opportunity to understand the nature of the X-ray plasma in DNe and the WD properties of this source. In this paper, we present the analysis results of *NICER* and *NuSTAR* data of MASTER J0302 taken during the outburst. To detect supersoft X-rays from the boundary layer is unfeasible for conventional X-ray detectors for monitoring use since most of which are sensitive only in hard X-rays above ~ 1 keV, and since large X-ray satellites seldom respond to alerts for outburst events in a timely manner. On the other hand, *NICER* is suitable for detecting the transient supersoft X-ray emission because it covers an energy range down to 0.2 keV and is well capable of flexible observations of transients. Hard X-ray observations with *NuSTAR* are also important to investigate the emission from the optically-thin coronal flow that coexists with the boundary layer even during outbursts (Wada et al. 2018; Kimura et al. 2021). This paper is organized as follows. Section 2 describes the X-ray observations. Section 3 shows our analysis results of light curves and spectra. We give our interpretation of the object and its X-ray radiation mechanism in section 4.

Throughout this paper, we assume the binary mass ratio $q = 0.063$ and the inclination angle $i = 60 \pm 10$ deg for MASTER J0302 on the basis of the analysis of the optical data (Tampo et al. in prep). We also assume the distance to the source $d = 720$ pc (Kato 2022), which was determined from the disk component at the superhump as a standard candle and has an uncertainty of $\sim 23\%$.

2. OBSERVATIONS AND ANALYSES

2.1. *NICER*

NICER monitored MASTER J0302 during its 2021–2022 outburst, starting 1.6 days after the epoch of the optical maximum. The observation IDs (ObsIDs) of the monitoring are given in Table A1 in the appendix section. In this work, we use HEASoft version 6.30.1 for data reduction and analyses. The data were reprocessed with the pipeline tool *nicer12*, which used the *NICER* Calibration Database (CALDB) version later than 2021 July 20, for producing light curves and time-averaged spectra. The light curves were generated by *lcurve*. The source and background spectra were extracted with *nibackgen3C50* version 7. *NICER* is composed of 56

modules of silicon drift detectors (SDDs), 52 of which are operating on orbit, including two noisy modules, IDs 14 and 34. In our data reduction with *nicer12*, we filtered out the data of the noisy two modules. For spectral analyses, we obtained the response matrix file and the ancillary response file for a specific set of 50 detectors to match the default settings of the background model.¹ All of the observation times were converted to barycentric Julian date (BJD) by *barycorr*.

2.2. *NuSTAR*

The *NuSTAR* Target of Opportunity (ToO) observations were carried out only on 2021 December 2. The observation log is given in Table A2. The observed area was partially overlapped with that of the *NICER* observation of ObsID 4202450104 on the same day. The data were reprocessed with *nupipeline* and the *NuSTAR* CALDB as of 2021 October 20. The light curves, time-averaged spectra, and response and ancillary response files were obtained with *nuproducts*. The background region was circular with a radius of $62''$ at a blank sky area. We determined the circular source region centered at the target position with a $25''$ radius.

3. RESULTS

3.1. *Light curves and variability*

The ultraviolet (UV), optical, and X-ray light curves are displayed in Figure 1. The optical light curves clearly show that the outburst lasted for ~ 2 months. The outburst amplitude was ~ 10 mag, which was unusually large in comparison with those of normal WZ Sge-type DNe, though there are several WZ Sge-type systems that exhibited outbursts with >9 -mag amplitudes (Kato 2015; Tampo et al. 2020). Using the same method described in section 2.1 of Dubus et al. (2018), we derived the mass accretion rate (\dot{M}_{acc}) of the disk onto the WD to be $\dot{M}_{\text{acc}} \sim 10^{19} \text{ g s}^{-1}$ ($\approx 2 \times 10^{-7} M_{\odot} \text{ yr}^{-1}$) to reproduce $V = 12$ mag, the observed brightest optical magnitude of the source (top panel of Figure 1), assuming the standard disk with a uniform accretion rate over the entire disk, $R_{\text{disk}} = 3 \times 10^{10} \text{ cm}$, $M_1 = 1.2 M_{\odot}$, and $R_{\text{in}} = 5 \times 10^8 \text{ cm}$, where R_{disk} and R_{in} are the radii of the outer and inner disk edges, respectively. Here, we assume that R_{disk} reached the 2:1 resonance radius (Osaki & Meyer 2002). The estimated accretion rate is higher than predicted for normal WZ Sge-type outbursts (Osaki 1995), which would be attributed to the high-amplitude outburst.

¹ The method is described at <https://heasarc.gsfc.nasa.gov/docs/nicer/analysis/rmf/>, and we use the additional data version xti20200722.

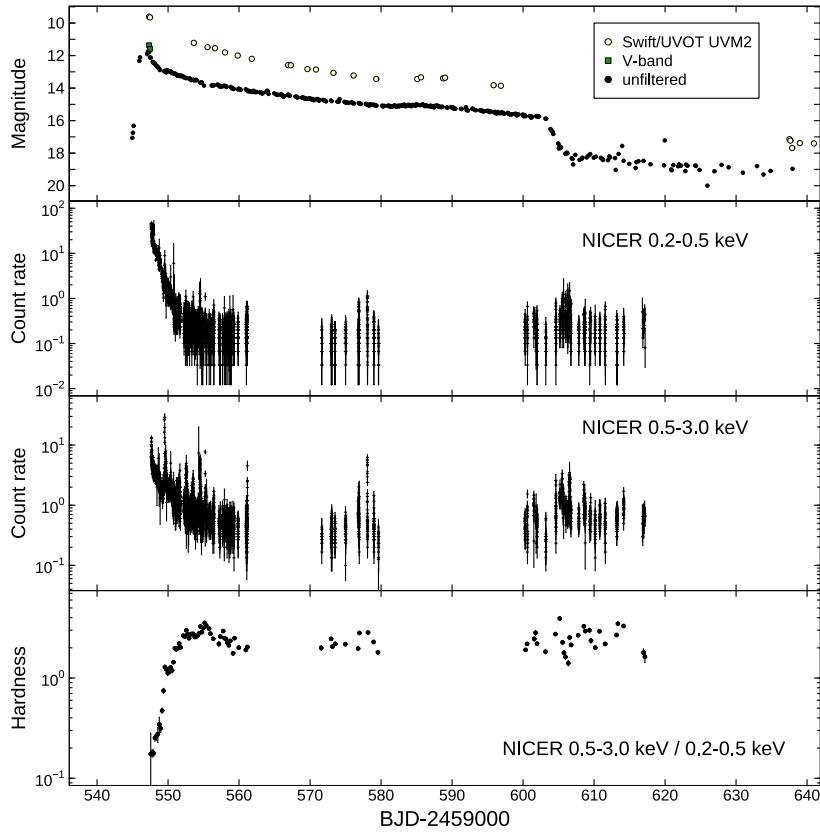


Figure 1. UV, optical, and X-ray light curves of the 2021–2022 outburst of MASTER J0302 for the entire observation period. Top panel shows the optical (green squares) *V*-band, (black filled circles) unfiltered, and (white open circles) *Swift* UM2-band data. The Variable Star Network (VSNET) team provides the optical data. The central wavelength of the *Swift* UM2-band is 2246 Å. The second and third panels show *NICER* X-ray light curves binned into 30-s bins in the 0.2–0.5 keV and 0.5–3.0 keV bands, respectively. Bottom panel shows the hardness ratio, the 0.5–3.0 keV count rate divided by the 0.2–0.5 keV count rate.

The decline rate of optical light curves is consistent with those of other WZ Sge-type DNe (Kato 2015). The decline of the UV light curve was similar to that of the optical light curve. The *NICER* observation started on 2021 November 28 (BJD 2459547), 1.6 d after the optical outburst maximum. The observed X-ray flux was highest at 3.8×10^{-11} ergs $s^{-1} cm^{-2}$ in the 0.2–3.0 keV when the observations started and then it rapidly declined. Considering the uncertainty of the distance to MASTER J0302, the optical and X-ray luminosities are less than 4.6×10^{35} ergs s^{-1} and 9.3×10^{34} ergs s^{-1} , respectively, which are about three orders of magnitude lower than the Eddington luminosity. This suggests that thermonuclear runaway on the WD surface is unlikely to have occurred at this object. The X-ray flux declined faster than the optical one and decreased by 70% and 30% per day in the 0.2–0.5 keV and 0.5–3.0 keV bands, respectively, till BJD 2459551. The hardness ratio of the fluxes between these two energy ranges, i.e., (0.5–3.0 keV)/(0.2–0.5 keV), rapidly increased as the X-ray fluxes decreased before it became stable eventually.

The X-ray light curve appears to have some spiky, potentially flaring, events (second and third panels of Figure 1). However, they are likely to originate from background fluctuations (see also Figure A2), as we found that each of the spiky events was synchronized with a sharp increase in the rate of the so-called “overshoot” events in *NICER*. Overshoot events are background events caused by a number of charges deposited along their traveling paths in the *NICER* SDD when high-energy charged particles, such as cosmic rays, enter the SDD².

3.2. Time-dependent X-ray spectra

The broadband X-ray spectrum was taken on BJD 2459551 by *NICER* and *NuSTAR*. First, we fitted the spectra with the model `Tbabs*pcfabs*(bbody+gaussian+gaussian+bremstrahlung)` in the XSPEC software (Arnaud 1996), where `Tbabs`, `pcfabs`, `bbody`, `gaussian`, and `bremstrahlung` denote

² For more details about the *NICER* overshoot event, see https://heasarc.gsfc.nasa.gov/docs/nicer/analysis_threads/overshoot-intro/

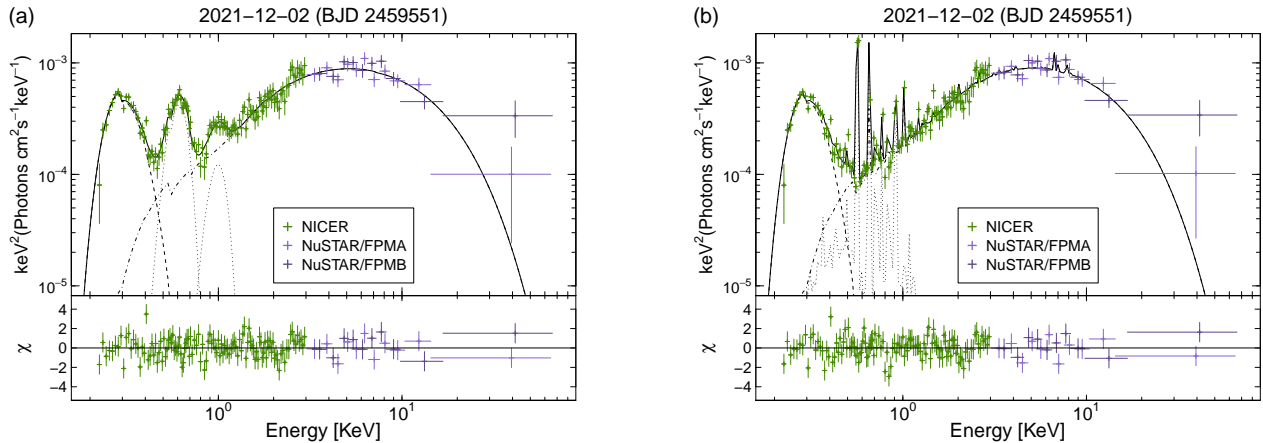


Figure 2. Broad-band X-ray SEDs of MASTER J0302 on BJD 2459551 (2021 December 2) during the outburst, overlaid with the best-fit spectral models of (a) $Tbabs*pcfabs*(bbody+gaussian+gaussian+bremstrahlung)$ and (b) $Tbabs*pcfabs*(bbody+vapec+vapec)$. Green crosses represent the *NICER* data. Purple and dark purple crosses represent the *NuSTAR* FPMA and FPMB data, respectively. In panel (a), dashed line and dot-dashed line represent the best-fit model components of blackbody and bremsstrahlung, respectively, and the two dotted lines do those of the oxygen and neon lines. Similarly, in panel (b), dashed line, dotted line, and dot-dashed line represent those of blackbody, low-temperature and high-temperature collisionally-ionized plasma emissions, respectively. Solid line in each panel shows the total best-fit model emission. The normalizations of the *NuSTAR* SED were 0.81 and 0.90 of the *NICER* SED for the data in panels (a) and (b), respectively.

X-ray absorption by the interstellar medium, partial-covering fraction for the absorption of X-rays, blackbody radiation, a single Gaussian model typically representing an emission line, and optically-thin bremsstrahlung radiation, respectively. The cross-normalization factor between the *NICER* and *NuSTAR* spectral energy distributions (SEDs) was corrected in the fitting. The result is exhibited in the left panel of Figure 2. Another form of plot for the same result is given in the left panel of Figure A3, in which the y-axis is the normalized count rate. We did not use the *NICER* spectrum above 3.0 keV because the estimated background rate of 0.1 counts s^{-1} keV $^{-1}$ at 3.0 keV was comparable to the observed count rate at the energy and it was even smaller at a higher energy. The column density N_H was fixed at 7.3×10^{20} cm $^{-2}$ in the *Tbabs* model; the value had been determined through simultaneous model-fitting of several *NICER* SEDs with a common N_H and is consistent with the galactic absorption to the direction of MASTER J0302.

We found that the spectrum is composed of three components; a blackbody component with a temperature of 30 ± 1 eV, two possible emission lines with non-negligible widths at around 0.6 and 1.0 keV, and bremsstrahlung radiation with a temperature of ~ 7 keV. Table 1 tabulates the best-fit parameters. The two broad lines are possibly blended lines emitted from helium-like and hydrogen-like ions of oxygen and neon, respectively, which *NICER* cannot resolve. Reportedly, the helium-like oxygen emission line in GW Lib, a WZ Sge-type DN, which was strong during the quiescence

state, disappeared during its outburst (Byckling et al. 2009; Hilton et al. 2007). The present result provides the first detection of strong oxygen and neon lines during an outburst in a DN. Complex iron emission lines at around 6.5 keV that are prominent in several DNe (Ishida et al. 2009; Wada et al. 2017; Perna et al. 2003; Szkody et al. 2002) were not detected during the outburst in MASTER J0302; the lack of detection is consistent with past observations of GW Lib and WZ Sge during the early stage of outbursts (Patterson et al. 1998; Hilton et al. 2007; Byckling et al. 2009). We estimated the upper limit of the iron-line flux from MASTER J0302 to be 10^{-13} erg s^{-1} cm $^{-2}$ by performing the modeling of simulated spectra. Here, we generated the simulated *NuSTAR* spectra in the ≥ 3 keV band with the *fakeit* command in *XSPEC* on the basis of the model $Tbabs*(bremstrahlung+gaussian)$, where the *gaussian* model represents the iron emission line at 6.5 keV, and investigated the strength of the iron line to determine how strong it could be observed.

We also performed another spectral modeling with the model $Tbabs*pcfabs*(bbody+vapec+vapec)$. Here, *vapec* represents the radiation from a collisionally-ionized diffuse gas on the basis of the *AtomDB* database for atomic parameters. The parameters of oxygen, neon, and iron abundances for the two *vapec* components were assumed to be the same for each element and the abundances of other elements than these three were fixed at the solar values. The right panel of Figure 2 and Table 1 show the fitting result and best-fit parameters, respectively. The result implied that the oxygen and

Table 1. Best-fit parameters for models of (a) $T_{\text{babs}}*p_{\text{cfabs}}*(b_{\text{body}}+g_{\text{aussian}}+g_{\text{aussian}}+b_{\text{remsstrahlung}})$ and (b) $T_{\text{babs}}*p_{\text{cfabs}}*(b_{\text{body}}+v_{\text{aprec}}+v_{\text{aprec}})$ in the simultaneous spectral model-fitting of the simultaneous *NICER* and *NuSTAR* observation data of MASTER J0302 on BJD 2459551 (2021 December 2). The errors represent 90% confidence ranges.

Model	Parameter	(a)	(b)
pcfabs	N_{H}^*	$2.7^{+1.0}_{-1.7}$	$1.7^{+1.1}_{-0.6}$
	f^\dagger	$0.62^{+0.05}_{-0.09}$	$0.61^{+0.06}_{-0.07}$
bbody	T_{BB}^\ddagger	$30^{+1.0}_{-0.5}$	30 ± 1.1
	L_{BB}^\S	1.5 ± 0.4	$1.3^{+0.5}_{-0.3}$
gaussian 1	E_1^\P	0.59 ± 0.006	–
	σ_1^\lrcorner	$6.0^{+1.0}_{-0.7}\times 10^{-2}$	–
	N_1^{**}	$7.4^{+1.3}_{-1.5}$	–
gaussian 2	E_2^\P	0.98 ± 0.03	–
	σ_2^\lrcorner	$5.5^{+3.0}_{-2.9}\times 10^{-2}$	–
	N_2^{**}	$5.0^{+7.7}_{-2.2}\times 10^{-1}$	–
vaprec 1	$kT_1^{\dagger\dagger}$	–	$0.18^{+0.01}_{-0.01}$
	$Z_{\text{O}}^{\ddagger\dagger}$	–	$5.8^{+5.9}_{-3.1}$
	$Z_{\text{Ne}}^{\S\S}$	–	$12^{+12}_{-6.8}$
	$Z_{\text{Fe}}^{\P\P}$	–	≤ 0.34
	$N_1^{\lrcorner\lrcorner}$	–	$1.3^{+1.4}_{-0.6}\times 10^{-4}$
bremsstrahlung	$T_{\text{brems}}^{\dagger\dagger}$	$6.7^{+1.0}_{-0.9}$	–
	N_3^{***}	$8.6^{+1.0}_{-0.9}\times 10^{-4}$	–
vaprec 2	$kT_2^{\dagger\dagger}$	–	$6.3^{+0.9}_{-0.8}$
	$N_2^{\lrcorner\lrcorner}$	–	$1.5^{+0.6}_{-0.4}\times 10^{-3}$
χ^2/dof		1.08	1.14

*Equivalent hydrogen column in 10^{22} atoms cm^{-2} .

† Dimensionless covering fraction ($0 < f \leq 1$).

‡ Temperature in eV.

¶ Blackbody luminosity in units of 10^{34} ergs s^{-1} .

§ Line energy in keV.

$^\lrcorner$ Line width in keV.

**Total photons/ cm^2/s in the line of sight in units of 10^{-4} .

†† Plasma temperature in keV.

‡† Oxygen abundance with respect to the solar one.

¶¶ Neon abundance with respect to the solar one.

§§ Iron abundance with respect to the solar one.

$^{\lrcorner\lrcorner}$ $\frac{10^{-14}}{4\pi(D_{\text{A}}(1+z))^2} \int n_e n_{\text{H}} dV$, where D_{A} is the angular distance to the source (cm), dV is the volume element (cm^3), and n_e and n_{H} are the electron and hydrogen densities (cm^{-3}), respectively.

*** $\frac{3.02\times 10^{-15}}{4\pi D^2} \int n_e n_{\text{I}} dV$, where D is the distance to the source (cm).

neon abundances were ~ 3 -times and ~ 5 -times of their solar abundances, respectively, whereas the X-ray emitting plasma in most DNe has sub-solar abundances for oxygen and neon (Pandel et al. 2005).

Next, we investigated the time evolutions of the blackbody component and oxygen and neon emission lines by model-fitting the *NICER* data at individual epochs, collectively spanning for 3.5 days, with the first of the above-used model,

$T_{\text{babs}}*p_{\text{cfabs}}*(b_{\text{body}}+g_{\text{aussian}}+g_{\text{aussian}}+b_{\text{remsstrahlung}})$.

In the fitting, due to the statistics limitation, we fixed the bremsstrahlung temperature, central energies and widths of the emission lines, and partial-absorption parameters at the best-fit values in Table 1. We note that the bremsstrahlung temperature of ~ 7 keV could be hardly constrained with this model-fitting of the *NICER* data alone because its data above 3.0 keV were dominated by the background and because no *NuSTAR*

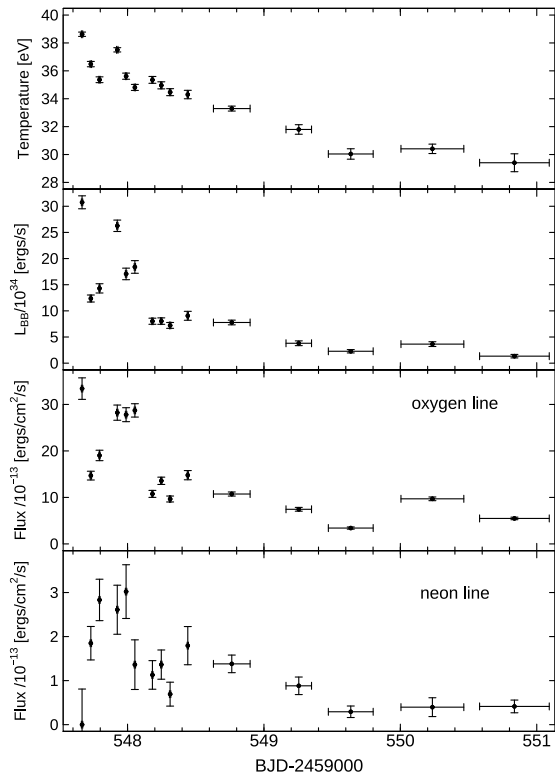


Figure 3. Time evolution of the blackbody radiation, oxygen and neon emission lines from MASTER J0302. Top and second panels show the time evolutions of the temperature and luminosity, respectively, of the blackbody component. The fourth and bottom panels show the time evolutions of the fluxes of the oxygen and neon lines, respectively. The line fluxes are corrected for absorption. The errors are in 90% confidence.

data were available other than those on BJD 2459551. Figure 3 shows the obtained time evolutions of the temperature and luminosity of the blackbody component, and the fluxes of oxygen and neon emission lines.

Notice from Figure 2 that the luminosity of the blackbody component exceeded 10^{35} ergs s^{-1} on BJD 2459547 and then decreased with time. The blackbody temperature ranged between 30–40 eV till BJD 2459551 and then decreased with time. The temperature during the outburst was a few times higher than those in other DNe. The blackbody flux declined faster than the neon and oxygen line fluxes. There is a clear difference in the observed decline rates between the two energy bands and that explains the rapid time evolution of the hardness ratio at the early stage of the outburst (bottom panel of Figure 1). The absorption-corrected oxygen and neon line luminosities were as strong as a few times 10^{32} and 10^{31} ergs s^{-1} , respectively, around BJD 2459547 in MASTER J0302, whereas they were known to be less than 10^{29} ergs s^{-1} in other DNe (Perna et al. 2003; Szkody et al. 2002).

4. DISCUSSION

4.1. X-ray properties of MASTER J0302 as a dwarf nova

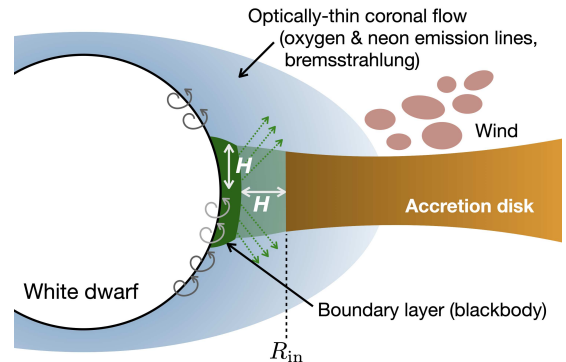


Figure 4. Schematic illustration of the accretion flow in the vicinity of the WD surface in MASTER J0302 in the edge-on view. Blue, green, and orange regions represent the high-temperature coronal flow observed in hard X-rays, the optically-thick boundary layer (with a scale height of H) observed in EUV and soft X-rays, and the low-temperature accretion disk observed at UV and optical wavelengths, respectively. The gas at the WD surface may leak to X-ray emitting plasma. Winds (red regions) may be blowing from the accretion disk and obscure part of soft X-rays emitted from the system.

The X-ray observational characteristics of MASTER J0302 are basically consistent with those observed in the past from other DNe during outbursts, though some unusual features were detected. Figure 4 displays the schematic picture of the X-ray emitting plasma in this source. CVs are broadly categorized into two groups according to the strength of the magnetic field of the WD: either strongly or weakly magnetized. We consider that this object is a non-magnetic CV because no significant periodicity originating from the WD rotation was found. If MASTER J0302 harbored a WD with a strong magnetic field, short-term periodic variations would be detected due to column accretion onto the spinning WD (Mauche 2006; Kennedy et al. 2017).

In the widely-accepted model, the X-ray emitting region in a DN exists in the vicinity of the WD, and it becomes optically thick (“boundary layer”) during outbursts and emits supersoft X-rays of blackbody radiation with a temperature of several tens of eV (see Introduction). It is usually difficult to detect a soft X-ray blackbody component with such a low temperature in DNe during outbursts. There have been a limited number of successful EUV and soft X-ray detections from this kind of objects, for example OY Car and U Gem (Long et al. 1995; Mauche & Raymond 2000;

Byckling et al. 2009). In this study, we used *NICER*, and successfully detected a low-temperature blackbody emission mere 1.6 days after the optical maximum, which had a temperature of ~ 30 eV and a luminosity of $\sim 10^{34}$ erg s $^{-1}$, in MASTER J0302 (see Figure 2). The observed luminosity is consistent with that from the boundary layer predicted by a theoretical model of Ferland et al. (1982).

Soft X-rays from the boundary layer in the WD system irradiate the inner part of the disk and drive outflows (Figure 4). The outflow feature is often observed to be imprinted in the UV spectroscopy of DNe during outbursts (Froning et al. 2001; Long et al. 2003). Our spectral analyses revealed dense gas with N_{H} of $\sim 10^{22}$ cm $^{-2}$ absorbing soft X-rays partially covering the X-ray emitting region, which may represent outflows and agrees with the general model of DNe (Figure 4). Also, our results suggest that a multi-temperature optically-thin coronal flow coexisted with an optically-thick boundary layer, the feature of which were observed in other DNe with high mass-accretion rates (Dobrotka et al. 2017; Byckling et al. 2009). The oxygen and neon emission lines, as we detected in MASTER J0302, are also likely to originate from the optically-thin corona.

However, the following observed characteristics are unusual for DNe.

- The oxygen and neon lines were very strong. The estimated abundances of oxygen and neon are at least a few times higher than their solar values.
- The radius of the blackbody emitter was as small as $\sim 4 \times 10^7$ cm, and the blackbody temperature was as high as ~ 30 eV.

4.2. Possible cause of prominent oxygen and neon emission lines

The X-ray emitting plasma in MASTER J0302 was much richer in oxygen and neon than that in other DNe (right column of Table 1). There are several possible hypotheses to explain the high abundances. One possibility is (A) the WD core is enriched with oxygen and neon, i.e., an ONe WD, and another possibility is (B) the secondary star provides oxygen and neon-rich gas to the boundary layer via the disk accretion. Although we cannot completely rule out the latter case (B), it seems highly unlikely because the secondary star is either a red dwarf or a brown dwarf (Hillman & Gerbi 2022).

Let us discuss the former case (A) as follows. In CVs in general, the difference in velocity between the accreted matter and the matter on the WD surface is expected to induce the Kelvin-Helmholtz instability, which stirs matter at the boundary between the WD surface

and the X-ray emitting plasma. However, the WD surface is covered by the accreted matter enriched with hydrogen. The boundary layer does not obtain oxygen and neon-rich gas through the above-mentioned process without recent nova eruptions, even if the WD core contains gas enriched with these two elements.

If a nova eruption occurs, the material of the WD core should be dredged up. If the WD core is enriched with oxygen and neon, the gas enriched with these two elements will be ejected and pollute the X-ray emitting plasma, the disk, and the secondary star. Since oxygen and neon-rich gas is not produced by the nuclear burning at the hydrogen-rich layer covering the WD, it should originate from the WD core (Hachisu & Kato 2016). A recent nova eruption may form a nova shell, though it was not detected in around half of novae and its time evolution has a rich variety (Downes & Duerbeck 2000; Tappert et al. 2020). The lack of high-resolution images of specific emission lines sensitive to nova shells prevents us from searching for nova shells. The possibility of a past nova eruption, therefore, still remains. We estimate the amounts of oxygen and neon gas on BJD 2459551 to be $\sim 8 \times 10^{15}$ g and $\sim 3 \times 10^{15}$ g, respectively, by using the best-fit values of the X-ray spectral modeling in section 3.2, which are much smaller than the ejected mass at one nova eruption. In this estimation, we assume that the X-ray emitting plasma is spherical with a radius of 10^9 cm. The amount of mass ejected from a massive WD at one nova eruption is $\sim 10^{-7}$ to $10^{-5} M_{\odot}$, and its ~ 1 – 10% is regarded to be the gas enriched with oxygen and neon (Prialnik & Kovetz 1995; Yaron et al. 2005; Hachisu & Kato 2016). It may not be surprising that the small amount of oxygen and neon-rich gas accreted from polluted gas in the disk and secondary star. To distinguish (A) and (B), we have to estimate the metallicity of the gas on the WD surface by UV spectroscopy. To investigate whether a nova shell exists or not, we have to perform high-resolution X-ray/UV/optical imaging. These observations and estimations are beyond the scope of this paper.

4.3. Possible evidence for a massive white dwarf

The following discussion is based on the hypothesis that the high abundances of oxygen and neon originate from the WD gas. The idea that MASTER J0302 has an ONe WD seems to be consistent with the compactness of its WD. Under the assumption that X-rays from the boundary layer are radiated from the surface of a belt-shaped region around the equatorial plane of the WD (see the green region and arrows in Figure 4), we estimated the WD radius (R_1) from the quantities determined by the SED modeling according to the following

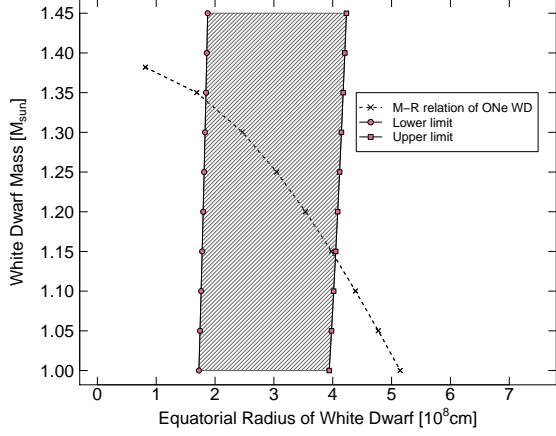


Figure 5. Relation between the mass and radius of the ONe WD. Dashed line with crosses represents the equatorial radius of the ONe WD with no rotation, as calculated by Kashiyama et al. (2019) (see also Figure 2 and text in the paper for details). The solid line with circles and that with squares are the lower and upper limits, respectively, of the WD mass as a function of the disk inner-edge radius for MASTER J0302, which are calculated according to equation (4) and observed quantities. The shaded region shows the possible range of the WD mass of MASTER J0302.

relation:

$$4\pi R_1 H = \frac{L_{\text{BB}}}{\sigma T_{\text{BB}}^4}, \quad (1)$$

where σ is the Stefan-Boltzmann constant and H is the scale height of the boundary layer, which is defined as the vertical extent from the equatorial plane to the surface (see Figure 4). Also, L_{BB} and T_{BB} denote the luminosity and temperature of the blackbody emitter, respectively. Here, we postulate that the radial extent of the boundary layer is $\sim H$ (Frank et al. 2002). Since the inclination angle of this object is less than 70 deg, the boundary layer is not eclipsed by the disk. An approximate analytic formula of H is given by

$$\left(\frac{H}{R}\right)^2 = 6.96 \times 10^{-4} \left(\frac{M_1}{0.7M_\odot}\right)^{-0.85} \left(\frac{\dot{M}_{\text{acc}}}{10^{18} \text{ g/s}}\right)^{0.22} + 7.29 \times 10^{-4} \left(\frac{M_1}{0.7M_\odot}\right)^{0.8} \left(\frac{\dot{M}_{\text{acc}}}{10^{18} \text{ g/s}}\right)^{1.0}, \quad (2)$$

where $R = R_1$ (see equation (2) in Patterson & Raymond 1985b). The accretion rate onto the WD, \dot{M}_{acc} , is calculated with

$$L_{\text{BB}} = \frac{GM_1 \dot{M}_{\text{acc}}}{2R_1} \text{ [ergs/s]}, \quad (3)$$

where G is the gravitational constant. Using equations (1), (2), and (3), we derive the mass-radius relation of

the WD to be

$$1.52 \times 10^{-6} \left(\frac{R_1}{10^8 \text{ cm}}\right)^{4.22} \left(\frac{M_1}{0.7M_\odot}\right)^{-1.07} \left(\frac{L_{\text{BB}}}{10^{34} \text{ erg/s}}\right)^{-0.78} + 7.97 \times 10^{-8} \left(\frac{R_1}{10^8 \text{ cm}}\right)^5 \left(\frac{M_1}{0.7M_\odot}\right)^{-0.2} = \left(\frac{L_{\text{BB}}}{10^{34} \text{ erg/s}}\right) \left(\frac{T_{\text{BB}}}{10^5 \text{ K}}\right)^{-8}. \quad (4)$$

The observed quantities on BJD 2459551 are $L_{\text{BB}} = (1.7 \pm 1.1) \times 10^{34} \text{ erg s}^{-1}$ and $T_{\text{BB}} = (3.5 \pm 0.1) \times 10^5 \text{ K}$, where the quoted errors are the combined ones for the 90% confidence intervals of the distance to the source and the estimates from the SED modeling (Table 1). We applied these values to equation (4) and obtained the possible range of R_1 for the given mass M_1 , which is displayed in Figure 5. Combining the range with the theoretical mass-radius relation of the ONe WD with no rotation (e.g., Kashiyama et al. 2019), we conclude that the possible range of the WD mass in MASTER J0302 is 1.15–1.34 M_\odot (Figure 5). The theoretical mass-radius relation is known not to vary significantly as long as the spin period of the WD is longer than 10 s, which is usually the case for CVs (Long et al. 2003; Yuasa et al. 2016). Hence, the uncertainty in applying the theoretical relation to our source should be limited.

The estimated mass is ~ 1.5 -times heavier than the average WD mass in CVs, $\sim 0.8 M_\odot$ (Littlefair et al. 2008; Savoury et al. 2011). We note that the actual WD mass may be even larger than this value. If we have overestimated the radiation efficiency of X-rays in equation (3), equation (4) is modified and the possible range on the WD radius-mass plane (shaded area in Figure 5) would shift toward the lower radius. This leads to a higher mass in conjunction with the theoretical mass-radius relation, which is a decreasing function of the radius R_1 . The temperature T_{BL} of the optically thick boundary layer is approximated as

$$T_{\text{BL}} = 2.16 \times 10^5 \left(\frac{M_1}{0.7M_\odot}\right)^{0.86} \left(\frac{\dot{M}_{\text{acc}}}{10^{18}}\right)^{0.18} \text{ [K]}, \quad (5)$$

(see equation (3) Patterson & Raymond 1985b), and positively correlated with the WD mass. The hypothesis that MASTER J0302 has a massive WD may naturally explain the observed high blackbody temperature.

Our analyses suggest that the WD in MASTER J0302 is an ONe WD with a mass very close to the Chandrasekhar mass. If the WD mass is larger than $1.32M_\odot$, the secondary star must be heavier than $0.08M_\odot$ according to the assumed mass ratio (see Introduction). The mass transfer rate from the secondary

star is $\sim 10^{-10} M_{\odot} \text{ yr}^{-1}$ (Kalomeni et al. 2016). In this case, the WD in this source may become a neutron star through an accretion-induced collapse (AIC) event within $\sim \text{Gyr}$ (see Wang & Liu 2020, and references therein), providing that the ONe WD grows due to the accretion from the secondary star. Then, after the AIC event, the system will likely become a binary system composed of a rapidly-rotating neutron star and a very light companion star, which is similar to a black-widow pulsar (Fruchter et al. 1988).

The number of the discovered WZ Sge-type DNe is still limited. However, a significant observation bias is likely to be present because the typical outburst interval of WZ Sge-type DNe is ~ 10 years (Kato 2015) and they would not be found during quiescence. Indeed, in the standard binary evolution scenario of CVs, WZ Sge-type DNe are the majority of the CV population (Knigge et al. 2011; Kalomeni et al. 2016). The yet undiscovered population of WZ Sge-type DNe may contribute to the birth-rate of the binary system consisting of a millisecond pulsar and a low-mass star (Tauris et al. 2013). The observed space density of WZ Sge-type DNe is $\sim 10^{-6} \text{ pc}^{-3}$ (Pala et al. 2020). Currently, there are no WZ Sge-type systems except for MASTER J0302, in which we find observational evidence of a massive ONe WD. The fraction of the objects like MASTER J0302 to WZ Sge-type DNe is at least $\sim 1/300$. The event rate of AIC from MASTER J0302-like objects is roughly estimated as $\sim 10^{-5} \text{ yr}^{-1} \text{ gal}^{-1}$. This may account at least a fraction for the theoretically-predicted birth rate of millisecond pulsars (Hurley et al. 2010).

5. CONCLUSIONS

MASTER J0302 exhibited an outburst in 2021–2022. This object was identified as a WZ Sge-type DN by detection of early and ordinary superhumps and double-peaked emission lines at the early stage of its outburst, though the outburst amplitude was ~ 10 mag, extremely high (see section 3.1). We analyzed the X-ray data taken with *NICER* and *NuSTAR*. The observed maximum X-

ray luminosity was $\sim 10^{35} \text{ erg s}^{-1}$. The *NICER* soft-X-ray observations enabled us to detect a blackbody component with a temperature of $\sim 30 \text{ eV}$ and a luminosity of $\sim 10^{34} \text{ erg s}^{-1}$ around the outburst maximum, which rapidly declined. This was interpreted as the emission from the optically-thick boundary layer. Also, the bremsstrahlung emission with a temperature of $\sim 7 \text{ keV}$ would originate from the optically-thin gas remaining even in outbursts. The partial absorption of soft X-rays by dense gas with N_{H} of $\sim 10^{22} \text{ cm}^{-2}$ implies that outflows from the disk covered the X-ray emitting plasma (see sections 3.2 and 4.1). These observational features were consistent with WZ Sge-type DNe; however, prominent oxygen and neon emission lines were extraordinary. It is unlikely that the secondary star provided oxygen and neon-rich gas. The enrichment could be associated with past nova eruptions if the central WD is an ONe WD, though this is still in debate (section 4.2). We estimated the WD mass from the luminosity and temperature of a blackbody component originating from the boundary layer to be as heavy as $1.15\text{--}1.34 M_{\odot}$. The system might evolve to a binary including a millisecond pulsar via AIC within another $\sim \text{Gyr}$ (section 4.3).

ACKNOWLEDGMENTS

M. Kimura acknowledges support by the Special Postdoctoral Researchers Program at RIKEN. We are thankful to Dr. Masaaki Sakano for his English proofreading. We are grateful to the many amateur observers in VSNET for providing the optical light curve presented in this paper. We acknowledge Dr. Keisuke Isogai who took optical spectra presented in this paper. This work was financially supported by Japan Society for the Promotion of Science Grants-in-Aid for Scientific Research (KAKENHI) Grant Numbers JP20K22374 (MK), JP21K13970 (MK), JP20K04010 (KK), JP20H01904 (KK), JP22H00130 (KK), JP22K03688 (TS), JP22K03671 (TS), JP20H05639 (TS), JP21J22351 (YT). We thank the anonymous referee for helpful comments.

REFERENCES

- Ahumada, R., Allende Prieto, C., Almeida, A., et al. 2020, *ApJS*, 249, 3, doi: [10.3847/1538-4365/ab929e](https://doi.org/10.3847/1538-4365/ab929e)
- Arnaud, K. A. 1996, in *Astronomical Society of the Pacific Conference Series*, Vol. 101, *Astronomical Data Analysis Software and Systems V*, ed. G. H. Jacoby & J. Barnes, 17
- Ayala, H. 2021, *The Astronomer’s Telegram*, 15079, 1
- Bednarek, W., & Śmiałkowski, A. 2022, *MNRAS*, 511, 3339, doi: [10.1093/mnras/stac243](https://doi.org/10.1093/mnras/stac243)
- Boettcher, M., Fu, M., Govenor, T., King, Q., & Roustazadeh, P. 2022, arXiv e-prints, arXiv:2204.12242, <https://arxiv.org/abs/2204.12242>
- Byckling, K., Osborne, J. P., Wheatley, P. J., et al. 2009, *MNRAS*, 399, 1576

- Dobrotka, A., Ness, J. U., Mineshige, S., & Nucita, A. A. 2017, *MNRAS*, 468, 1183, doi: [10.1093/mnras/stx513](https://doi.org/10.1093/mnras/stx513)
- Downes, R. A., & Duerbeck, H. W. 2000, *AJ*, 120, 2007
- Dubus, G., Otulakowska-Hypka, M., & Lasota, J.-P. 2018, *A&A*, 617, A26, doi: [10.1051/0004-6361/201833372](https://doi.org/10.1051/0004-6361/201833372)
- Ferland, G. J., Langer, S. H., MacDonald, J., et al. 1982, *ApJL*, 262, L53, doi: [10.1086/183910](https://doi.org/10.1086/183910)
- Frank, J., King, A., & Raine, D. J. 2002, *Accretion Power in Astrophysics: Third Edition*
- Froning, C. S., Long, K. S., Drew, J. E., Knigge, C., & Proga, D. 2001, *ApJ*, 562, 963, doi: [10.1086/32386010.48550/arXiv.astro-ph/0107463](https://doi.org/10.1086/32386010.48550/arXiv.astro-ph/0107463)
- Fruchter, A. S., Stinebring, D. R., & Taylor, J. H. 1988, *Nature*, 333, 237, doi: [10.1038/333237a0](https://doi.org/10.1038/333237a0)
- Guetta, D., Hillman, Y., & Della Valle, M. 2023, *JCAP*, 2023, 015, doi: [10.1088/1475-7516/2023/03/015](https://doi.org/10.1088/1475-7516/2023/03/015)
- Hachisu, I., & Kato, M. 2016, *ApJ*, 816, 26, doi: [10.3847/0004-637X/816/1/26](https://doi.org/10.3847/0004-637X/816/1/26)
- Hillman, Y., & Gerbi, M. 2022, *MNRAS*, 511, 5570, doi: [10.1093/mnras/stac432](https://doi.org/10.1093/mnras/stac432)
- Hilton, E. J., Szkody, P., Mukadam, A., et al. 2007, *AJ*, 134, 1503
- Hurley, J. R., Tout, C. A., Wickramasinghe, D. T., Ferrario, L., & Kiel, P. D. 2010, *MNRAS*, 402, 1437, doi: [10.1111/j.1365-2966.2009.15988.x](https://doi.org/10.1111/j.1365-2966.2009.15988.x)
- Ishida, M., Okada, S., Hayashi, T., et al. 2009, *PASJ*, 61, 77
- Isogai, K., Tampo, Y., Yamanaka, M., et al. 2021, *The Astronomer's Telegram*, 15074, 1
- Kadler, M., Eppel, F., Hessdoerfer, J., et al. 2021, *The Astronomer's Telegram*, 15076, 1
- Kalomeni, B., Nelson, L., Rappaport, S., et al. 2016, *ApJ*, 833, 83, doi: [10.3847/1538-4357/833/1/83](https://doi.org/10.3847/1538-4357/833/1/83)
- Kashiyama, K., Fujisawa, K., & Shigeyama, T. 2019, *ApJ*, 887, 39, doi: [10.3847/1538-4357/ab4e97](https://doi.org/10.3847/1538-4357/ab4e97)
- Kato, T. 2015, *PASJ*, 67, 108, doi: [10.1093/pasj/psv077](https://doi.org/10.1093/pasj/psv077)
- . 2022, arXiv e-prints, arXiv:2202.02956. <https://arxiv.org/abs/2202.02956>
- Kennedy, M. R., Garnavich, P. M., Littlefield, C., et al. 2017, *MNRAS*, 469, 956, doi: [10.1093/mnras/stx880](https://doi.org/10.1093/mnras/stx880)
- Kimura, M., Yamada, S., Nakaniwa, N., et al. 2021, *PASJ*, 73, 1262, doi: [10.1093/pasj/psab073](https://doi.org/10.1093/pasj/psab073)
- Knigge, C., Baraffe, I., & Patterson, J. 2011, *ApJ*, 194, 28
- Kulkarni, S. R., & Narayan, R. 1988, *ApJ*, 335, 755, doi: [10.1086/166964](https://doi.org/10.1086/166964)
- Kurita, M., Kino, M., Iwamuro, F., et al. 2020, *PASJ*, 72, 48, doi: [10.1093/pasj/psaa036](https://doi.org/10.1093/pasj/psaa036)
- Lagunas, C. 2021, *GRB Coord. Netw. Circ.*, 31126
- Littlefair, S. P., Dhillon, V. S., Marsh, T. R., et al. 2008, *MNRAS*, 388, 1582
- Long, K. S., Froning, C. S., Gänsicke, B., et al. 2003, *ApJ*, 591, 1172
- Long, K. S., Mauche, C. W., Szkody, P., & Mattei, J. 1995, in *Cataclysmic Variables*, ed. A. Bianchini, M. della Valle, & M. Orio, 133
- Matsubayashi, K., Ohta, K., Iwamuro, F., et al. 2019, *PASJ*, 71, 102, doi: [10.1093/pasj/psz087](https://doi.org/10.1093/pasj/psz087)
- Mauche, C. W. 2004, *ApJ*, 610, 422, doi: [10.1086/421438](https://doi.org/10.1086/421438)
- . 2006, *MNRAS*, 369, 1983
- Mauche, C. W., & Raymond, J. C. 2000, 9, 232
- Narayan, R., & Popham, R. 1993, *Nature*, 362, 820, doi: [10.1038/362820a0](https://doi.org/10.1038/362820a0)
- Neustroev, V. V., Page, K. L., Kuulkers, E., et al. 2018, *A&A*, 611, A13, doi: [10.1051/0004-6361/201731719](https://doi.org/10.1051/0004-6361/201731719)
- Osaki, Y. 1995, in *Cataclysmic Variables*, ed. A. Bianchini, M. della Valle, & M. Orio, 307
- Osaki, Y. 1996, *PASP*, 108, 39
- . 2005, 81, 291
- Osaki, Y., & Meyer, F. 2002, *A&A*, 383, 574
- Pala, A. F., Gänsicke, B. T., Breedt, E., et al. 2020, *MNRAS*, 494, 3799, doi: [10.1093/mnras/staa764](https://doi.org/10.1093/mnras/staa764)
- Paliya, V. S. 2021, *The Astronomer's Telegram*, 15073, 1
- Pandel, D., Córdova, F. A., Mason, K. O., & Priedhorsky, W. C. 2005, *ApJ*, 626, 396, doi: [10.1086/429983](https://doi.org/10.1086/429983)
- Patterson, J., & Raymond, J. C. 1985a, *ApJ*, 292, 535
- . 1985b, *ApJ*, 292, 550
- Patterson, J., Richman, H., Kemp, J., & Mukai, K. 1998, *PASP*, 110, 403
- Perna, R., McDowell, J., Menou, K., Raymond, J., & Medvedev, M. V. 2003, *ApJ*, 598, 545
- Prialnik, D., & Kovetz, A. 1995, *ApJ*, 445, 789, doi: [10.1086/175741](https://doi.org/10.1086/175741)
- Quinn, J., VERISTAS Collaboration, Metzger, B., & Sokoloski, J. 2021, *The Astronomer's Telegram*, 15078, 1
- Sarneczky, K., Vinko, J., & Kiss, L. 2021, *The Astronomer's Telegram*, 15081, 1
- Savoury, C. D. J., Littlefair, S. P., Dhillon, V. S., et al. 2011, *MNRAS*, 415, 2025, doi: [10.1111/j.1365-2966.2011.18707.x](https://doi.org/10.1111/j.1365-2966.2011.18707.x)
- Stein, R., Karambelkar, V., Kasliwal, M. M., et al. 2021, *The Astronomer's Telegram*, 15069, 1
- Szkody, P., Nishikida, K., Seth, A., et al. 2002, in 261, *The Physics of Cataclysmic Variables and Related Objects*, ed. B. T. Gänsicke, K. Beuermann, & K. Reinsch, 75
- Tampo, Y., Naoto, K., Isogai, K., et al. 2020, *PASJ*, 72, 49, doi: [10.1093/pasj/psaa043](https://doi.org/10.1093/pasj/psaa043)
- Tappert, C., Vogt, N., Ederoclite, A., et al. 2020, *A&A*, 641, A122, doi: [10.1051/0004-6361/202037913](https://doi.org/10.1051/0004-6361/202037913)
- Tauris, T. M., Sanyal, D., Yoon, S. C., & Langer, N. 2013, *A&A*, 558, A39, doi: [10.1051/0004-6361/201321662](https://doi.org/10.1051/0004-6361/201321662)

- Wada, Q., Tsujimoto, M., Ebisawa, K., & Hayashi, T. 2017, PASJ, 69, 10, doi: [10.1093/pasj/psw114](https://doi.org/10.1093/pasj/psw114)
- Wada, Y., Yuasa, T., Nakazawa, K., et al. 2018, MNRAS, 474, 1564, doi: [10.1093/mnras/stx2880](https://doi.org/10.1093/mnras/stx2880)
- Wang, B., & Liu, D. 2020, Research in Astronomy and Astrophysics, 20, 135, doi: [10.1088/1674-4527/20/9/135](https://doi.org/10.1088/1674-4527/20/9/135)
- Warner, B. 1995, Cataclysmic Variable Stars
- Wheatley, P. J., & Mauche, C. W. 2005, in Astronomical Society of the Pacific Conference Series, Vol. 330, The Astrophysics of Cataclysmic Variables and Related Objects, ed. J. M. Hameury & J. P. Lasota, 257. <https://arxiv.org/abs/astro-ph/0412166>
- Yaron, O., Prialnik, D., Shara, M. M., & Kovetz, A. 2005, ApJ, 623, 398, doi: [10.1086/428435](https://doi.org/10.1086/428435)
- Yuasa, T., Hayashi, T., & Ishida, M. 2016, MNRAS, 459, 779, doi: [10.1093/mnras/stw734](https://doi.org/10.1093/mnras/stw734)
- Zhirkov, K., Kechin, Y., Lipunov, V., et al. 2021, The Astronomer's Telegram, 15067, 1

APPENDIX

A. SUPPLEMENTARY TABLES AND FIGURES

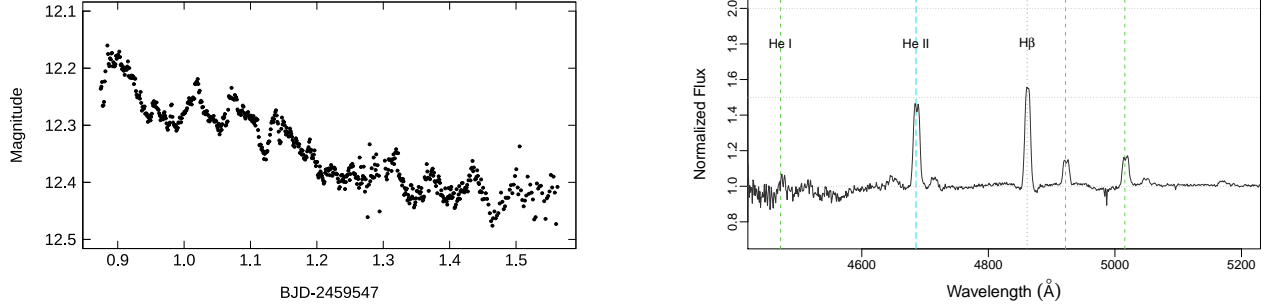


Figure A1. (Left) An example of light curves of early superhumps during the 2021–2022 outburst of MASTER J0302, whose period is identical with the orbital period (Tampo et al. in prep.). (Right) An example of optical spectra in which double-peaked emission lines are dominant on BJD 2459547 (Isogai et al. 2021). This was taken by Kyoto Okayama Optical Low-dispersion Spectrograph with an Integral Field Unit (KOOLS-IFU; Matsubayashi et al. (2019)) mounted on the 3.8-m telescope Seimei at Okayama Observatory, Kyoto University (Kurita et al. 2020). The blue dot, green dashed, and cyan dashed lines represent the central wavelength of Balmer, He I, and He II lines, respectively.

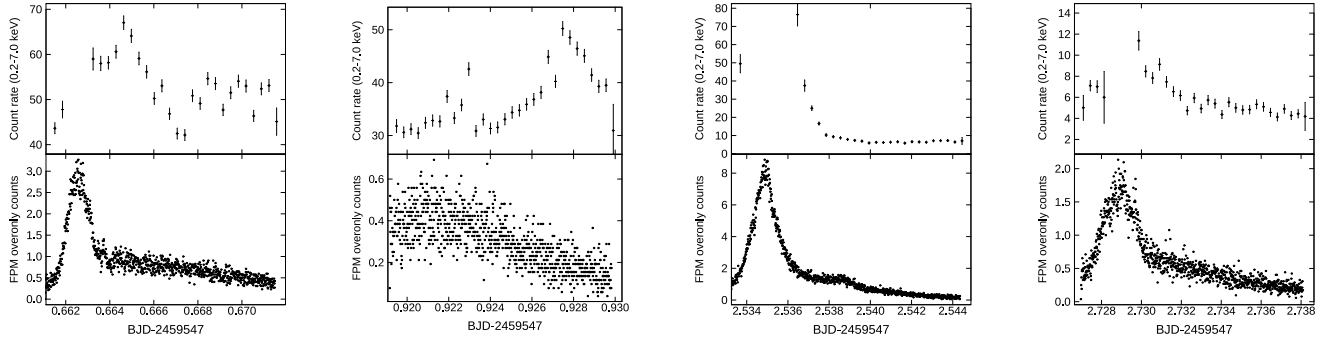


Figure A2. Examples of X-ray variability in the 2021–2022 outburst of MASTER J0302. The upper and lower panels of each figure denote the *NICER* count rate in the 0.2–7.0 keV and FPM overonly count which represents the average per-detector overshoot rate, respectively. Most of flares seemed to be caused by charged particles. When high energy charged particles such as cosmic rays pass through the *NICER* SDDs, many charges deposited in SDDs along its path are registered as an overshoot event. The flare in the second figure from the left seemed to be intrinsic to MASTER J0302 because there is no flare in FPM overonly count, and was dominant in the softer energy range.

Table A1. Log of observations of MASTER J0302 with *NICER*.

NICER ObsID	Start*	End*	On-source time [†]	Average rate [‡]
4202450101	547.6613	548.4464	8181	13.8
4202450102	548.6296	549.4791	5199	5.9
4202450103	549.5335	550.4653	9169	3.9
4202450104	550.5297	551.4982	9432	1.9
4202450105	551.5373	552.4495	4538	1.6
4202450106	552.5053	553.4805	10101	1.4
4202450107	553.5360	554.4495	8154	1.1
4202450108	554.5045	555.4348	9116	1.0
4202450109	555.7957	556.4547	3716	0.9
4202450110	557.1680	557.3630	2446	0.7
4202450111	557.6674	558.3249	3938	0.7
4202450112	558.5711	559.2946	5933	0.7
4202450113	559.8632	559.8779	1267	0.7
4202450114	561.0258	561.1776	5714	0.7
4202450117	571.6462	571.6506	375	0.5
4202450118	572.9937	573.0676	1754	0.5
4202450119	573.5130	573.5213	712	0.5
4202450120	574.9912	575.0070	1369	0.6
4202450121	576.7971	576.9312	2247	1.0
4202450122	578.0803	578.0951	1211	0.8
4202450123	578.9859	579.0042	1571	0.7
4202450124	579.6328	579.6470	667	0.4
4202450125	600.2890	600.2986	833	0.7
4202450126	600.6161	600.6252	789	0.5
4202450127	601.5152	601.9802	1842	0.9
4202450128	603.2009	603.2064	470	0.6
4202450129	604.6126	605.2021	1681	1.8
4202450130	605.5150	606.4878	3069	1.6
4202450131	606.5463	606.7459	1693	1.5
4202450132	607.8387	607.8476	774	0.9
4202450133	608.5486	609.3911	2338	1.4
4202450134	609.5164	610.1706	1109	0.8
4202450135	610.8065	610.8207	1219	1.0
4202450136	611.5806	611.5934	1094	0.8
4202450137	613.1933	613.2737	2706	1.0
4202450138	614.1603	614.1702	851	1.8
4202450139	616.8054	617.1925	260	0.9

*BJD–2459000.0.

[†]Units of seconds.[‡]*NICER* count rate in 0.3–7 keV in units of counts/sec.

Table A2. Log of observations of MASTER J0302 with *NuSTAR*.

NuSTAR ObsID	Start*	End*	On-source time [†]	Average rate [‡]
90701341002	550.4917	551.2005	36218	0.4

*BJD–2459000.0.

[†]Units of seconds.

[‡]NuSTAR count rate in 3–79 keV in units of counts/sec.

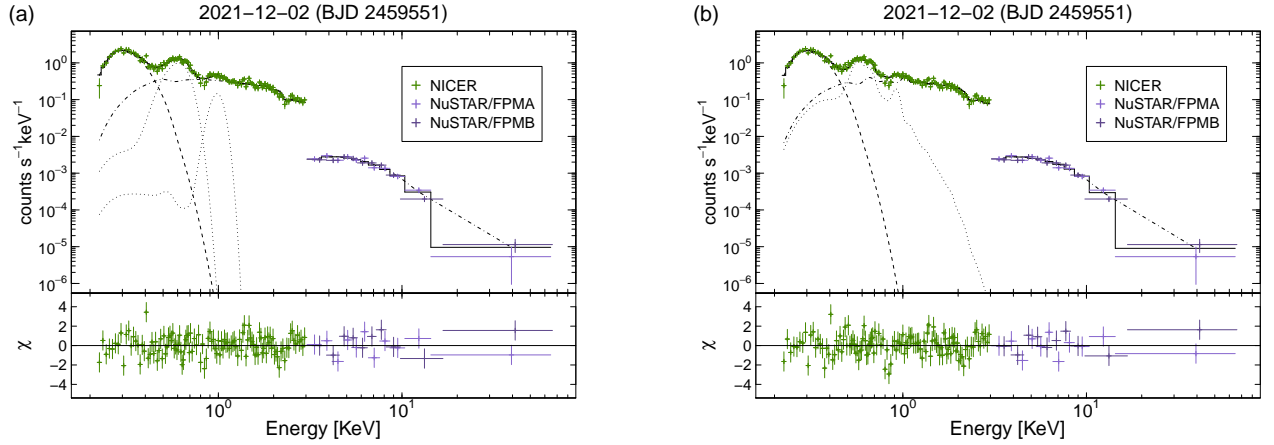


Figure A3. Broad-band X-ray data of MASTER J0302 on BJD 2459551 (2021 December 2) during the outburst. The green crosses represent the *NICER* data. The purple and dark purple crosses represent the *NuSTAR* FPMA and FPMB data, respectively. (a) The data with the best-fit spectral model of $Tbabs*pcfabs*(bbody+gaussian+gaussian+bremstrahlung)$. The dashed line and dot-dashed line represent the model emission from a blackbody source and that from bremsstrahlung source, respectively. The two dot lines denote the model emission from oxygen and neon lines. The solid line is a sum of the model emission. (b) The data with the best-fit spectral model of $Tbabs*pcfabs*(bbody+vapec+vapec)$. The dashed line, dot line, and dot-dashed line represent the model emission from a blackbody source, a low-temperature and a high-temperature collisionally-ionized plasma, respectively. The solid line is a sum of the model emission.